



HAL
open science

High-pressure Raman spectroscopy study of wurtzite ZnO

Frédéric Decremps, Julio Pellicer-Porres, A. Marco M Saitta, Jean-Claude Chervin, Alain Polian

► **To cite this version:**

Frédéric Decremps, Julio Pellicer-Porres, A. Marco M Saitta, Jean-Claude Chervin, Alain Polian. High-pressure Raman spectroscopy study of wurtzite ZnO. *Physical Review B: Condensed Matter and Materials Physics* (1998-2015), 2002, 65 (9), 10.1103/PhysRevB.65.092101 . hal-01921305

HAL Id: hal-01921305

<https://hal.sorbonne-universite.fr/hal-01921305>

Submitted on 13 Nov 2018

HAL is a multi-disciplinary open access archive for the deposit and dissemination of scientific research documents, whether they are published or not. The documents may come from teaching and research institutions in France or abroad, or from public or private research centers.

L'archive ouverte pluridisciplinaire **HAL**, est destinée au dépôt et à la diffusion de documents scientifiques de niveau recherche, publiés ou non, émanant des établissements d'enseignement et de recherche français ou étrangers, des laboratoires publics ou privés.

High pressure Raman spectroscopy study of Wurtzite ZnO

F. Decremps, J. Pellicer-Porres^a, A. M. Saitta, J.-C. Chervin and A. Polian
Physique des Milieux Condensés, CNRS-UMR 7602, Université Pierre & Marie Curie,
B77, 4, place Jussieu, 75252 Paris CEDEX 05, France

(Dated: November 13, 2018)

The high pressure behavior of optical phonons in wurtzite zinc oxide (*w*-ZnO) has been studied using room temperature Raman spectroscopy and *ab-initio* calculations based on a plane wave pseudopotential method within the density functional theory. The pressure dependence of the zone-center phonons (E_2 , A_1 and E_1) was measured for the wurtzite structure up to the hexagonal→cubic transition near 9 GPa. Above this pressure no active mode was observed. The only negative Grüneisen parameter is that of the E_2^{low} mode. E_1 (LO) and (TO) frequencies increase with increasing pressure. The corresponding perpendicular tensor component of the Born's transverse dynamic charge e_T^* is experimentally found to increase under compression like $e_T^*(P) = 2.02 + 6.4 \cdot 10^{-3} \cdot P$ whereas calculations give $e_T^*(P) = 2.09 - 2.5 \cdot 10^{-3} \cdot P$ (in units of the elementary charge e , P in GPa). In both cases, the pressure variation is small, indicating a weak dependence of the bond ionicity with pressure. The pressure dependence of the optical mode energies is also compared with the prediction of a model that treats the wurtzite-to-rocksalt transition as an homogeneous shear strain. There is no evidence of anomaly in the E_2 and A_1 modes behavior before the phase transition.

PACS numbers: PACS: 78.30.-j, 64.70.Dv, 91.60.GF

Zinc oxide belongs to the wide band-gap semiconductor family with large ionic characters of chemical bonds². The ionic size or relative electronegativity has been used to explain high pressure structure changes in $A^N B^{8-N}$ semiconductors. First principles calculations have shown that the zinc-blende (or wurtzite)→rocksalt→ β -Sn transition sequence is a common feature for most semiconductors. However, recent experimental identification of new intermediate phases (like cinnabar in CdTe for example) and the systematic absence of some phases (rocksalt (*rs*) for covalent compounds and β -Sn for all except the most covalent) invalidate the traditional transition sequence and, consequently, question the standard theoretical approach. In a recent Letter, Ozoliņš and Zunger³ suggested that phase transitions are accompanied by phonon softening, whose instability has to be taken into account in the calculation to correctly predict the phase diagram. The latter outcome can also be discussed in terms of the transition mechanism, where the presence of negative Grüneisen parameters of phonon modes may play an important role. Recently, a new intermediate structure has been proposed in the wurtzite to rocksalt transformation path of GaN, along which the optical A_1 and E_2^{high} modes are expected to be affected by the new bond formations⁴. Wurtzite ZnO, which transforms under pressure into the *rs* phase at 9 GPa, may provide a good example of this trend.

Wurtzite ZnO belongs to the C_{6v}^4 ($P6_3mc$) space group. The primitive cell includes two formula units, with all atoms occupying 2b sites of symmetry C_{3v} . At the Γ point of the Brillouin zone, group theory predicts the existence of the following optics modes: $\Gamma_{opt} = A_1 + 2B_1 + E_1 + 2E_2$. Frequency from the B_1^{low} and B_1^{high} silent modes has been calculated at 260 and 540 cm^{-1} respectively. A_1 , E_1 and E_2 modes are Raman active. In addition A_1 and E_1 are infrared active, and

therefore split into longitudinal and transverse components (LO and TO). The mode assignment at ambient conditions is well established in the literature⁵. To the best of our knowledge, no calculation and only two experimental attempts have been made to study the *w*-ZnO phonon frequency shift under pressure^{6,7}. In the first reference, the authors report the evolution of two phonon frequencies, E_2^{high} and E_2^{low} , over a relative small pressure range (0-1 GPa). In the second one, the pressure dependence of four Raman modes (E_2^{high} , E_2^{low} , A_1 (TO) and E_1 (TO)) are given up to ~ 7.5 GPa. However no experimental details is described, neither on the sample nor on the apparatus (high pressure cell, pressure transmitting medium or pressure measurement). This lack of information is detrimental to any discussion, especially in our case where, on compression at room temperature, non-hydrostatic stresses are known to affect considerably the phonon response of the crystal. Here, we report the results on the high pressure behaviour of optical phonons in *w*-ZnO from both Raman experiments and *ab-initio* calculations.

For the high pressure Raman experiments, two samples were cut as platelets from a large, colorless and transparent single-crystalline cube of *w*-ZnO purchased from SPC Goodwill. The sample was tailored to about $30 \times 20 \mu\text{m}^2$ surface and $20 \mu\text{m}$ thick. One crystal was polished with plane parallel surfaces normal to the hexagonal *c*-axis, and the other one with surfaces normal to the *a*-axis. The high pressure cell was a membrane diamond anvil cell (DAC)⁸. A stainless steel gasket was preindented to $50 \mu\text{m}$ and a $200 \mu\text{m}$ hole was drilled in the center by spark-erosion. Neon gas loaded at high pressure (0.15 GPa) was used as a pressure transmitting medium because : (i) it is hydrostatic up to 16 GPa⁹, (ii) it is chemically inert, (iii) it has no luminescence and no Raman activity. Pressure was systematically measured be-

fore and after each Raman spectra using the fluorescence emission of a ruby sphere¹⁰ placed close to the sample into the gasket hole. The accuracy was better than 0.1 GPa at the maximum pressure reached. Raman spectra were excited with the 514.5 nm line of an Ar⁺ laser focused down to 5 μm with a power level of about 500 mW at the entrance of the DAC. The scattered light was analyzed with a Dilor XY triple spectrometer and a liquid-nitrogen-cooled CCD multichannel detector. All spectra were recorded in the backscattering geometry with unpolarized light. In this geometry, E₂, A₁(TO) and E₁(TO) are allowed with incident radiation perpendicular to the *c*-axis, and E₂, A₁(LO) with light parallel to the *c*-axis. The Raman frequencies were determined from a computer fit of the peaks with a Lorentzian profile. The accuracy was better than 1 cm⁻¹.

Phonon frequencies, Born effective charges, and the dielectric constant ϵ_∞ have been calculated from first-principles in the framework of density-functional theory and local-density approximation, by using the PWSCF code¹¹. We adopted the density-functional perturbation theory (DFPT) approach¹² and a standard local-density approximation plane-wave/pseudopotential scheme. Norm-conserving pseudopotentials of the Troullier-Martins form¹³ have been used, with the inclusion of 3*d* electrons of Zn in the valence shell. Tests carried out with zinc 3*d* electrons in the core and non-linear core-correction gave an unsatisfactory accuracy on phonon frequencies. We used a cutoff of 70 Ry and a 8×8×4 mesh of special *k*-points for Brillouin zone integration. At each pressure, *w*-ZnO has been relaxed with respect to the $\frac{c}{a}$ ratio and the internal parameter *u*, and phonon frequencies have been calculated at these optimized structural parameters. Because of the polar character of ZnO, the dynamical matrix displays nonanalytic behavior in the limit $\mathbf{q} \rightarrow 0$, arising from the long-range character of the Coulomb forces. The calculations of LO modes is nonetheless straightforward, since the LO-TO splitting only depends on the phonon frequencies, the dielectric constant and the Born effective charges, which can all be directly calculated in the DFPT framework.

Before performing the high pressure experiment we examined the optical zone-center phonons of *w*-ZnO at ambient pressure with light parallel and perpendicular to the *c*-axis. We employed the large single crystal from which the micrometric samples used in the high pressure experiments were extracted. The E₂, A₁(TO) and E₁(TO) modes are clearly seen in the spectra. On the contrary, the A₁(LO) mode is hardly observable and not seen at high pressure (crystal in the DAC). The frequency assignment, as well as a comparison with *ab-initio* results and previous works, is presented in Table I. The Raman spectra in both configurations also show additional features at 331 and 552 cm⁻¹. In reference⁵ they are tentatively assigned to second order structures by comparison with flat regions in the dispersion curves.

Under pressure, with incidence parallel to the *c*-axis, only E₂ single phonon mode was apparent when focusing

TABLE I: Experimental and theoretical Raman-active *w*-ZnO Γ -point phonon frequencies (in cm⁻¹) at ambient conditions.

Mode	this work (exp.)	this work (theo.)	Ref. ¹⁴	Ref. ⁵
E ₂ ^{low}	99	92	101	101
E ₂ ^{high}	439	449	444	437
A ₁ (TO)	382	397	380	380
E ₁ (TO)	414	426	413	408
A ₁ (LO)	574	559	579	574
E ₁ (LO)	580	577	591	584

at the center of the sample. In the same configuration, A₁(TO), E₁(TO) and a new mode at 580 cm⁻¹ appear with the laser light focused on the sample border. The new mode is much more intense than the A₁(LO) found in ambient conditions. Its frequency is also slightly higher. The E₁(LO) mode is forbidden in the backscattering geometry. However, it has been observed in ZnO in the forbidden *X*(ZZ) \bar{X} geometry⁵. We have thus assigned the mode appearing at 580 cm⁻¹ to the E₁(LO) mode. Our assignment should be considered as tentative since the new mode is observed only when we focused on the sample border. In this situation, the incidence direction with respect to the crystal axes is not defined and mixed modes may be obtained. In that geometry, typical Raman spectra of ZnO at various pressures are shown in Fig. 1.

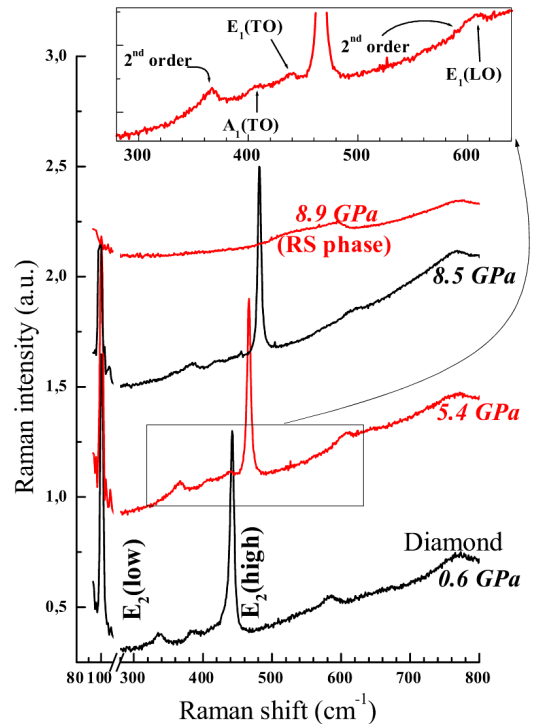


FIG. 1: Raman spectra of single-crystalline ZnO under different hydrostatic pressures in the backscattering geometry. The spectra are shifted upward for clarity.

TABLE II: ZnO mode Grüneisen parameters γ_i of the zone-center phonons

symmetry	this work (exp.)	this work (theo.)	Ref. ⁷
E_2^{low}	-1.6	-1.67	-1.75
E_2^{high}	2.0	1.84	1.62
$A_1(TO)$	2.1	1.70	1.70
$E_1(TO)$	1.8	1.80	1.76
$E_1(LO)$	1.4	1.30	-

The pressure dependence of the phonon frequencies for the two high-pressure runs are shown in Fig. 2. No difference between the two runs is observed. Around 8.7 GPa, the disappearance of all Raman peaks reflects the onset of the wurtzite-rocksalt structural transformation in excellent agreement with the previous high-pressure studies. E_2^{low} is the only mode which exhibit a negative pressure dependence. The frequency shift of E_2^{high} , $A_1(TO)$, $E_1(TO)$ and $E_1(LO)$ modes increase with pressure and no anomaly up to the transition pressure is detected. The frequency dependence of E_2^{low} and E_2^{high} are in perfect agreement with the low pressure values obtained from Mitra *et al*⁶. On the other hand, while our frequency data seem to agree with those of Minomura⁷ (except $A_1(TO)$), the discrepancy in the corresponding Grüneisen parameters is important (except for $E_1(TO)$, see Table II). It is difficult to account for that disagreement since no calculation details are given in Ref.⁷. We suspect the author to have used a different bulk modulus. Here, the mode Grüneisen parameters γ_i are defined as: $\gamma_i = -\left(\frac{d \ln \nu_i}{d \ln V}\right)_{P=0} = \frac{B_0}{\nu_i} \frac{d \nu_i}{d P}$. The isothermal Birch-Murnaghan equation of state was used to determine $B_0=170$ GPa and $B'=4$ from the X-ray diffraction data $V(P)$ ¹⁵.

The experimental LO-TO splitting of the E_1 phonon mode increases with a small pressure dependence (+2% at 5 GPa, see Fig. 2), in good agreement with theoretical results where no variation of the E_1 or A_1 LO-TO splitting is obtained in the same pressure range. It is noteworthy that this splitting increases (nearly constant from calculations) with pressure, an uncommon behavior for $A^N B^{8-N}$ semiconductors except SiC¹⁶, AlN and GaN¹⁷. The change of the Born's transverse dynamic charge e_T^* under compression can be determined from the measured frequencies using (in S.I. units): $(e_T^*)^2 = 4\pi^2 V \mu \epsilon_0 \epsilon_\infty (\nu_{LO}^2 - \nu_{TO}^2)$, where V is the volume per formula, μ is the reduced mass, ϵ_0 is the vacuum permittivity and ϵ_∞ is the high frequency (optical) dielectric constant¹⁸. At ambient pressure, and with $\epsilon_\infty(P=0)=3.95 \cdot \epsilon_0$, the experimental effective charge values are 2.02 and 2.4 (in units of the elementary charge e) for the E_1 and A_1 modes respectively. The evolution of the high frequency dielectric constant ϵ_∞ under high pressure has not been measured. To our knowledge only the dependence of the ordinary (n_o) and extraordinary (n_e) refractive indices at $0.5893 \mu\text{m}$ has been measured¹⁹.

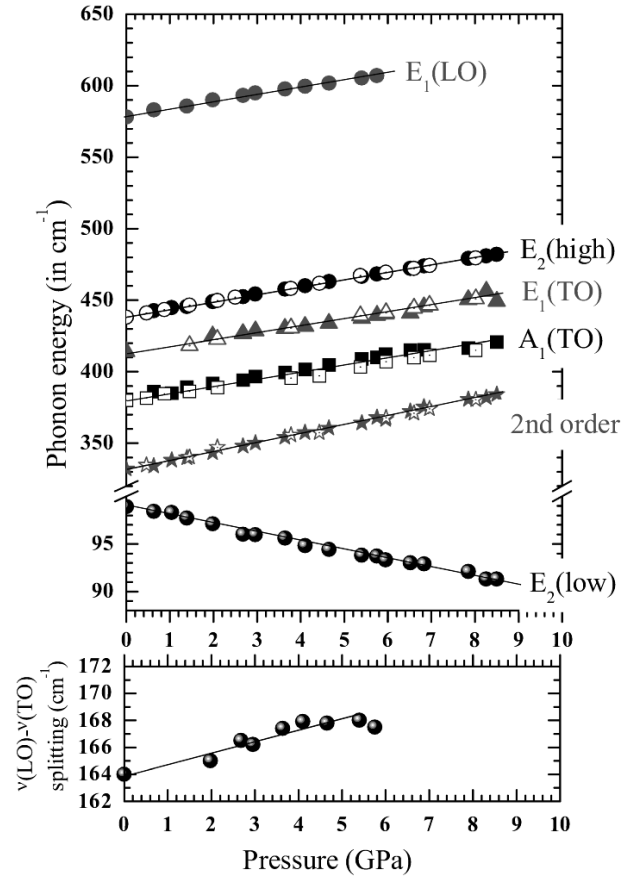


FIG. 2: Top: Pressure dependence of the observed optical phonons. Open (full) symbols: propagation of light perpendicular (parallel) to c . Bottom: $(\nu_{LO} - \nu_{TO}) E_1$ phonon mode splitting versus pressure. Solid lines are linear least-square fits to the experimental points.

In order to estimate the pressure behavior of e_T^* from our measurements, we suppose that the pressure dependence of ϵ_∞ and n_o^2 are equal. With this assumption, we obtain (in S.I. units): $\left(\frac{\partial \epsilon_\infty}{\partial P}\right)_{P=0} = 2n_o \left(\frac{\partial n_o}{\partial P}\right)_{P=0} = -0.014 \cdot \epsilon_0 \text{ GPa}^{-1}$. The behavior under pressure of the normalized perpendicular tensor component $e_T^*/e_T^*(0)$ is plotted in Fig. 3. The effective charge in w -ZnO increases under compression with $\partial e_T^*/\partial P = 6.4 \cdot 10^{-3}$ (in units of the elementary charge e per GPa). Theoretically, ϵ_∞ and the effective charge have been found to decrease linearly with pressure: $\left(\frac{\partial \epsilon_\infty}{\partial P}\right)_{P=0} = -0.025 \cdot \epsilon_0 \text{ GPa}^{-1}$ and $\partial e_T^*/\partial P = -2.5 \cdot 10^{-3}$. However, if we constrain the calculations to use the experimental pressure dependence of ϵ_∞ , we obtain $\partial e_T^*/\partial P \simeq 0$. These results may indicate a small variation of the w -ZnO bond ionicity when compressed between 0 and 4 GPa. In comparison, the $\partial e_T^*/\partial P$ experimental value for SiC¹⁶ is $5.3 \cdot 10^{-3}$, $0.15 \cdot 10^{-3}$ for AlN¹⁷ and $-1.3 \cdot 10^{-3}$ for GaN¹⁷. Above 4 GPa, Fig. 3 shows a saturation of e_T^* . However, the refractive indices (and thus the dielectric constant) have only been measured between 0 and ~ 1 GPa¹⁹, which means that our $e_T^*(P)$ values above that pressure range

have been obtained from an extrapolation of $\varepsilon_\infty(P)$.

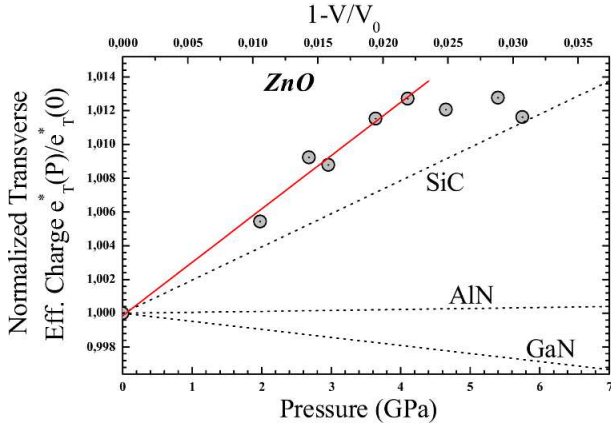


FIG. 3: Experimental pressure and volume dependence of the perpendicular component e_T^* under compression normalized to its ambient pressure value $e_T^*(0) = 2.02$. For comparison, dotted lines represent the experimental values of e_T^* for SiC¹⁶, AlN¹⁷ and GaN¹⁷.

We now turn the discussion to the simple homogeneous orthorhombic shear strain path proposed to picture the w to rs mechanism of transition⁴. This model predicts that under pressure, a relaxation of the structural parameter u from $\sim \frac{3}{8}$ up to $\frac{1}{2}$ is expected to occur in the wurtzite structure (*i.e.* below the phase transition) which gives rise to a new intermediate phase isomorphic to h -MgO. In addition to the expected (and experimentally observed) negative mode Grüneisen parameter of E_{2low}^2 at Γ , the previous model predicts the optic A_1 and E_2^{high} modes at Γ to be affected by the $w \rightarrow h$ -MgO transition. However, in the pressure range probed during the present work (from atmospheric up to the transition pressure, *i.e.* 9 GPa), no instability of these modes is observed. Our results show a discrepancy with the A_1 and E_1 anomaly expected from calculations and agree with the conclusions derived from long-range order probe (x-

ray diffraction experiments) by Desgreniers²⁰, where the evaluation of the normalized integrated intensity of the (002) and (101) diffraction lines indicated no deviation of the u parameter from its ideal value.

In summary, the LO-TO splitting of the E_1 phonon mode has been experimentally and theoretically found to be weakly pressure dependent. This unusual behavior is related to a small variation of the chemical bonds ionicity of w -ZnO with pressure. Moreover, the present observation of optical phonon under pressure does not show any softening of the optic A_1 and E_2^{high} modes as theoretically expected⁴. All Grüneisen parameters show positive values except that of E_2^{low} , which is a quite common feature in II-VI compounds. However, from first-principles calculation on w -ZnO, we predict (in good agreement with Ref.⁴) u parameter to shift up to 0.5 at a volume of 24.08 \AA^3 (*i.e.* ~ 21 GPa). Experimentally, the w -to- rs first-order transition limits the pressure range of w structure existence and, consequently, does not allow the second-order process observation (*via* optical phonons instabilities for example). However, if we refer to the phase diagram of ZnO²¹, it may be possible to constrain the structure to be still tetrahedrally coordinated at low temperature in order to make the wurtzite \rightarrow NaCl transition to occur at higher pressure, rendering the second-order process directly observable for the first time in semiconductors.

Acknowledgments

We wish to acknowledge Bernard Couzinet for the neon DAC loading. One of us (A.M.S.) acknowledges the Institut du Développement et des Ressources en Informatique Scientifique (IDRIS) for computer time allocation (project 11387-CP9). This research has been partly supported by a Marie Curie fellowship of the European Community number HPMF CT2000-00764.

^a Permanent address: *Institut de Ciència dels Materials, Universitat de València, Departamento de Física Aplicada, Edifici Investigació, E-46100 Burjassot (València), Spain*
² A. Garcia and M.L. Cohen, Phys. Rev. B **47**, 4215 (1993).
³ V. Ozoliņš and A. Zunger, Phys. Rev. Lett. **82**, 767 (1999).
⁴ S. Limpijumng and W.R.L. Lambrecht, Phys. Rev. Lett. **86**, 91 (2001); J. Serrano, A. Rubio, E. Hernández, A. Muñoz and A. Mujica, Phys. Rev. B **66**, 16612 (2000).
⁵ J.M. Calleja and M. Cardona, Phys. Rev. B **16**, 3753 (1977).
⁶ S.S. Mitra, O. Brafman, W.B. Daniels and R.K. Crawford, Phys. Rev. **186**, 942 (1969).
⁷ S. Minomura, *High Pressure in Science and Technology, Proceedings of the 9th AIRAPT International High Pressure Conference* (Elsevier Science Publishing Co., New York 1984) 277.

⁸ R. Letoullec, J.P. Pinceaux and P. Loubeyre, High Pressure Res. **1**, 77 (1988).
⁹ H. K. Mao, J. Xu and B. M. Bell, J. Geophys. Res. B **91**, 4673 (1986).
¹⁰ G.J. Piermarini, S. Block, J.D. Barnett, and R.A. Forman, J. Appl. Phys. **46**, 2774 (1975).
¹¹ PWSCF code: www.pwscf.org.
¹² S. Baroni, P. Giannozzi, and A. Testa, Phys. Rev. Lett. **58**, 1861 (1987); P. Giannozzi, S. de Gironcoli, P. Pavone, and S. Baroni, Phys. Rev. B **43**, 7231 (1991).
¹³ Troullier, N.; Martins, J.M., Phys. Rev. B **1991**, 43, 1993.
¹⁴ C.A. Arguello, D.L. Rousseau and S.P.S. Porto, Phys. Rev. **181**, 1351 (1969).
¹⁵ F. Decremps *et al*, to be published.
¹⁶ J. Liu and Y.K. Vohra, Phys. Rev. Lett. **72**, 4105 (1994); K. Karch and F. Bechstedt, Phys. Rev. Lett. **77**, 1660

- (1996).
- ¹⁷ A.R. Goñi, H. Siegle, K. Syassen, C. Thomsen and J.-M. Wagner, Phys. Rev. B **64**, 035205 (2001).
- ¹⁸ M. Born and K. Huang, Dynamical theory of crystal lattices (Clarendon, Oxford, 1954), chap. 2.
- ¹⁹ K. Vedam and T.A. Davis, Phys. Rev. **181**, 1196 (1969).
- ²⁰ S. Desgreniers, Phys. Rev. B **58**, 14102 (1998).
- ²¹ F. Decremps, J. Zhang and R. C. Liebermann, Eur. Phys. Lett. **51**, 268 (2000).